PROPORTIONAL–INTEGRAL–DERIVATIVE CONTROLLER FOR ARMED MANIPULATOR ROBOTS

Alaeddin Malek* and Farideh Giv*

Abstract

In this paper, torque controlling for one, two, and three armed manipulator robots by proportional–integral–derivative (PID) controller methods with different payloads are proposed. By giving the initial and final conditions, we first directly solve the dynamical system to determine the state containing position and velocity. Secondly, the appropriate PID controller coefficients are determined. Thirdly, the optimal torque by using PID controller coefficients is computed. Then the related position and velocity trajectories based on initial and final conditions are derived. Simulation for 100 work examples with different payloads and a various number of arms are considered. Numerical results for different types of armed robots (R, RR, RRR) for different loads are given. The graphs for position, velocity and optimal torque trajectories for 15 work examples and different payloads are depicted.

Key Words

Proportional–integral–derivative controller, armed manipulator robots, robot dynamics

1. Introduction

Robot manipulators have many applications, such as in manufacturing, aerospace and transportation[1]–[3]. Due to the highly coupled nonlinear dynamics and model uncertainties and external disturbances, the design of high-performance controlling robot manipulators is challenging and has attracted much attention in recent years [4]. Proportional–integral–derivative (PID) controller has been used widely due to its simplicity [5]–[8]. The integral control action in a PID controller is to achieve asymptotic regulation and disturbance rejection. While the derivative control action is to achieve a minimum rate of error [9]. In light of the well-known internal model principle, integral control can only effectively suppress the constant disturbances to achieve the asymptotic stability of the closed-loop systems [10]. However, for the system with model uncertainties and non-constant external disturbances, there are always residual errors using the PID controller, and asymptotic regulation cannot be achieved. In this article, PID controllers (see Section 3), are used to lift loads from 21.2 to 1000 g by armed robot manipulators [11]. The paper is organised as follows: In Section 2, systems dynamic for armed robots is proposed. The statement of the optimal control input is proposed for applied torque to the corresponding armed robots in Section 3. In Section 4, the problem is described. In Section 5 corresponding complicated systems of the differential equation for robot type R, RR, RRR is given. Numerical simulation and the corresponding results for 15 different examples are discussed and graphs for the position, velocity, and optimal torque are depicted. Concluding remarks are given in Section 6.

* Department of Applied Mathematics, Tarbiat Modares University, Tehran, Iran; e-mail: mala@modares.ac.ir; f.giiv@modares.ac.ir
Corresponding author: Alaeddin Malek

Recommended by Dan Zhang
(DOI: 10.2316/J.2024.206-0852)

2. Robot Dynamic System

Dynamic equations clearly explain the relationship between force and motion. Considering motion equations is important for robot design, simulation, robot motion animation and control algorithms. To describe the behaviour of dynamic systems, Euler–Lagrange equations are introduced. To determine the Lagrangian Euler equations, it is necessary to form the Lagrangian system, which is the difference between kinetic energy and potential energy [12].

Note that the kinetic energy of a rigid object is the sum of the transient kinetic energy and the rotational kinetic energy of the body around the center of mass. Also in terms of rigid dynamics, the only source of energy is gravity potential.

In this section, the Euler–Lagrange equations are investigated in a special case where the following two conditions are met. The first is that the kinetic energy is a quadratic function of the vector $\dot{q}$ and the second is that the potential energy is independent of $\dot{q}$. The arm robot has the following dynamic system [12]

$$D(q)\ddot{q} + C(q,\dot{q}) + g(q) = \tau \tag{1}$$

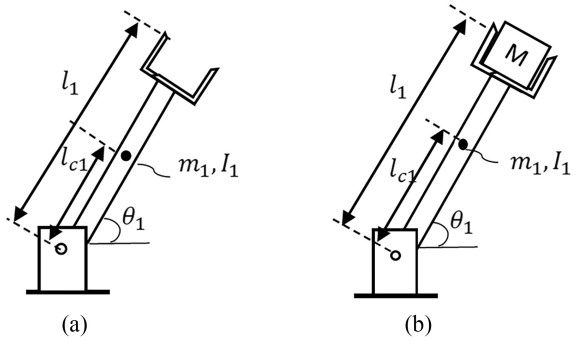

Figure 1. R robot manipulator: (a) without payload and (b) with payload M.

Table 1
Physical Characteristics for One-armed Robot Without Payload

Arm #	l_1	l_{c1}	m_1	I_1
	0.250 m	0.198 m	0.193 kg	1.15×10^{-3} kg.m^2

Table 2
Physical Characteristics of Two-armed Robot Without Payload

Arms #i	l_i	$l_{\rm ci}$	m_i	I_i
	0.250 m	0.198 m	0.193 kg	1.15×10^{-3} kg.m^2
	0.234 m	0.143 m	0.115 kg	4.99×10^{-4} kg.m^2

where τ is the generalised force associated with q. The variable q is also considered as generalised coordinates $(\theta_1, \theta_2, \ldots, \theta_n)$ that has n degrees of freedom. $g(q)$ is the gravity vector, $C(q, \dot{q})$ is the Christopher matrix and $D(q)$ is the inertia matrix [12]. This system consists of a typical second-order nonlinear differential equation (the number of equations corresponds to the number of arms).

2.1 One-armed Robot (R-type)

The physical characteristics for an R-type armed robot without payload are given in Table 1 [13]. For $i = 1, 2, 3$, l_i is the length of the i-th arm, $l_{\rm ci}$ is the i-th center of mass, m_i is the mass of the i-th arm and I_i is the i-th inertial torque.

According to (1) the dynamic system for one arm robot (see Fig. 1(a)) is

$$\tau_1 = (m_1 l_{c1}^2 + I_1)\ddot{\theta}_1 + m_1 g l_{c1} \cos(\theta_1) \qquad (2)$$

in which τ_1 is the corresponding torque for one-armed robot.

2.2 Two-armed Robots (RR-type)

The physical characteristics for RR-type robots without payload are given in Table 2 [13].

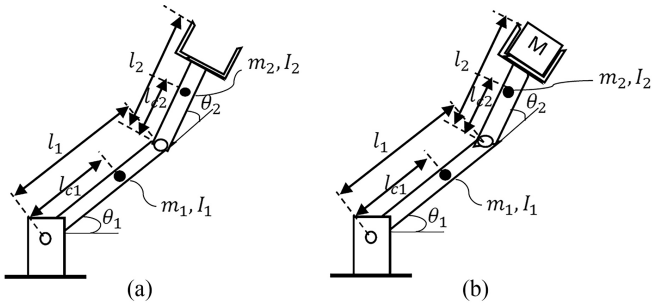

Figure 2. RR robot manipulator: (a) without payload and (b) with payload M.

Table 3
Physical Characteristics for Three-armed Robot Without Payload

Arms #i	l_i	$l_{\rm ci}$	m_i	I_i
	0.250 m	0.198 m	0.193 kg	1.15×10^{-3} kg.m^2
	0.234 m	0.143 m	0.115 kg	4.99×10^{-4} kg.m^2
	0.218 m	0.109 m	0.100 kg	6.58×10^{-4} kg.m^2

Form (1), the dynamic system for RR-type robot (see Fig. 2(a)) in matrix form is as follows [12]

$$\begin{pmatrix} \tau_1 \\ \tau_2 \end{pmatrix} = \begin{pmatrix} d_{11} & d_{12} \\ d_{21} & d_{22} \end{pmatrix} \begin{pmatrix} \ddot{\theta}_1 \\ \ddot{\theta}_2 \end{pmatrix} + \begin{pmatrix} h\dot{\theta}_2 & h\dot{\theta}_1 + h\dot{\theta}_2 \\ -h\dot{\theta}_1 & 0 \end{pmatrix} \begin{pmatrix} \dot{\theta}_1 \\ \dot{\theta}_2 \end{pmatrix} + \begin{pmatrix} g_1 \\ g_2 \end{pmatrix} \qquad (3)$$

where

$$\begin{aligned}
d_{11} &= m_1\, l_{c1}^2 + m_2\, (l_1^2 + l_{c2}^2 + 2\, l_1\, l_{c1}^2 + 2\, l_1\, l_{c2}\, \cos(\theta_2)) \\
&\quad + I_1 + I_2 0.1 \text{ cm} \\
d_{12} &= d_{21} = m_2\, (l_{c2}^2 + l_1\, l_{c2}\, \cos(\theta_2)) + I_2 0.1 \text{ cm} \\
d_{22} &= m_2\, l_{c2}^2 + I_2 0.1 \text{ cm} \\
c_{121} &= c_{211} = \frac{1}{2} \left(\frac{\delta d_{11}}{\delta \theta_2} \right) = -m_2\, l_1\, l_{c2} \sin(\theta_2) = h 0.1 \text{ cm} \\
c_{221} &= \left(\frac{\delta d_{12}}{\delta \theta_2} \right) - \frac{1}{2} \left(\frac{\delta d_{22}}{\delta \theta_1} \right) = h 0.1 \text{ cm} \\
c_{112} &= \left(\frac{\delta d_{21}}{\delta \theta_1} \right) - \frac{1}{2} \left(\frac{\delta d_{11}}{\delta \theta_2} \right) = -h 0.1 \text{ cm} \\
g_1 &= (m_1\, l_{c1} + m_2\, l_1)\, \text{g}\, \cos(\theta_1) \\
&\quad + m_2\, \text{g}\, l_{c2}\, \cos(\theta_1 + \theta_2) 0.1 \text{ cm} \\
g_2 &= m_2\, \text{g}\, l_{c2}\, \cos(\theta_1 + \theta_2).
\end{aligned}$$

2.3 Three-armed Robots (RRR-type)

As it is shown in Fig. 3, the physical characteristics of RRR-type robots without payload are given in Table 3.

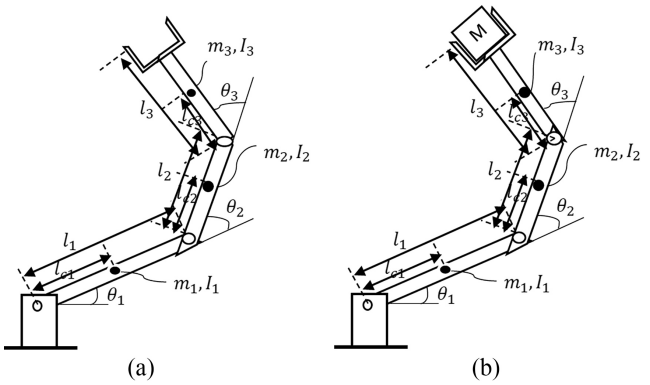

Figure 3. RRR robot manipulator: (a) without payload and (b) with payload M.

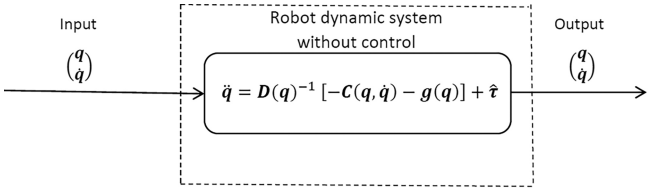

Figure 4. Block diagram of open-loop system without control.

According to (1) the dynamic system for RRR-type robot similar to (2) and (3) yields

$$\begin{pmatrix} \tau_1 \\ \tau_2 \\ \tau_3 \end{pmatrix} = \begin{pmatrix} d_{11} & d_{12} & d_{13} \\ d_{21} & d_{22} & d_{23} \\ d_{31} & d_{32} & d_{33} \end{pmatrix} \begin{pmatrix} \ddot{\theta}_1 \\ \ddot{\theta}_2 \\ \ddot{\theta}_3 \end{pmatrix} + \begin{pmatrix} c_{11} & c_{12} & c_{13} \\ c_{21} & c_{22} & c_{23} \\ c_{31} & c_{32} & c_{33} \end{pmatrix} \begin{pmatrix} \dot{\theta}_1 \\ \dot{\theta}_2 \\ \dot{\theta}_3 \end{pmatrix} + \begin{pmatrix} g_1 \\ g_2 \\ g_3 \end{pmatrix} \tag{4}$$

where appropriate c_{ij} and d_{ij}, $i, j = 1, 2, 3$ and g_i, $i = 1, 2, 3$ can be derived similar to the coefficients of RRR-type robot (see [14]). The block diagram of open-loop dynamical system corresponding to (2)–(4) is shown in Fig. 4.

3. Proportional–Integral–Derivative (PID) Controller

PID controller is a control system based on feedback, the main purpose of which is to bring the final result for the process closer to the desired value. Simply put, the whole concern of a PID controller is to steer the system towards a level, position, or whatever value we specify. In the PID controller, two definitions of error and setpoint are important. Setpoint here means the target point (level, position, quantity or whatever we want to reach in the control system) and on the other hand, the error is the amount of deviation (difference) between the target point and the final output value. The lower the error, the better, which means that we have been able to match the final value of the system exactly to our intended value. To achieve this desired point (error = zero, system output value = setpoint) PID controller system of three operators uses; Proportional (P), Integral (I), and Derivative (D) concepts. These three bases P, I and D are variable in the proposed PID controller to achieve the optimal response (torque). In practice, each of them takes the error signal ((e_1 = desired $position - position$) and (e_2 = desired $velocity - velocity$)) as input and performs an operation on it, and finally, their output is aggregated. As a torque (see Fig. 6), the output of this set, which is the output of the PID controller, is given to the feedback system to correct the error (see Fig. 5).

3.1 PID Definitions

The standard PID formula is as follows

$$\mathrm{output}(t) = k_p \left(e(t) + \frac{1}{T_i} \int_0^t e(\alpha)\, d\alpha + T_d\, \frac{\mathrm{de}}{\mathrm{dt}} \right) \tag{5}$$

where e stands for error, T_i is an integration time and T_d is a derivative time. Therefore, the conversion function $G(s)$ for the PID controller is [9]

$$G(s) = k_P + \frac{k_I}{s} + k_D\ \mathrm{s}, \tag{6}$$

in which s is the complex frequency. Proportional sentence "coefficient k_P" increases system speed and reduces "but does not zero" the permanent state differences to some extent. Adding an integral sentence "coefficient k_I" vanishes the permanent state differences, but adds a lot of overshoot to the transient response. The derivative sentence "coefficient k_D" attenuates the transient response fluctuations and brings the step response closer to the ideal desired [15].

3.2 Parallel PID

As it is stated in (6), the PID controller is called parallel since each action (P, I, and D) occurs in separate terms with the combined effect being a simple sum [16]. In the parallel equation, each action parameter (k_P, k_D, k_I) is independent of the others. Here, it is assumed that the gain parameter affects all three control actions.

4. Problem Description

The problem here is defined as the determination of the best possible control strategy (optimal control torque vector $\widehat{\tau}$), which minimises a performance index as the difference between of desired position and initial position for the top of the last arm. The last arm has a payload of mass M and the goal is to transport the mass M from the initial position into the desired position. The robot dynamic system under control is described in Section 2.

Observe that, this problem is not the minimum time control problem since the terminal time is fixed, here $\widehat{\tau}$, in which components of $\widehat{\tau}$ depend on three different types of robots. This problem can be called a fixed endpoint for a fixed time problem. Since the nonlinear problem here

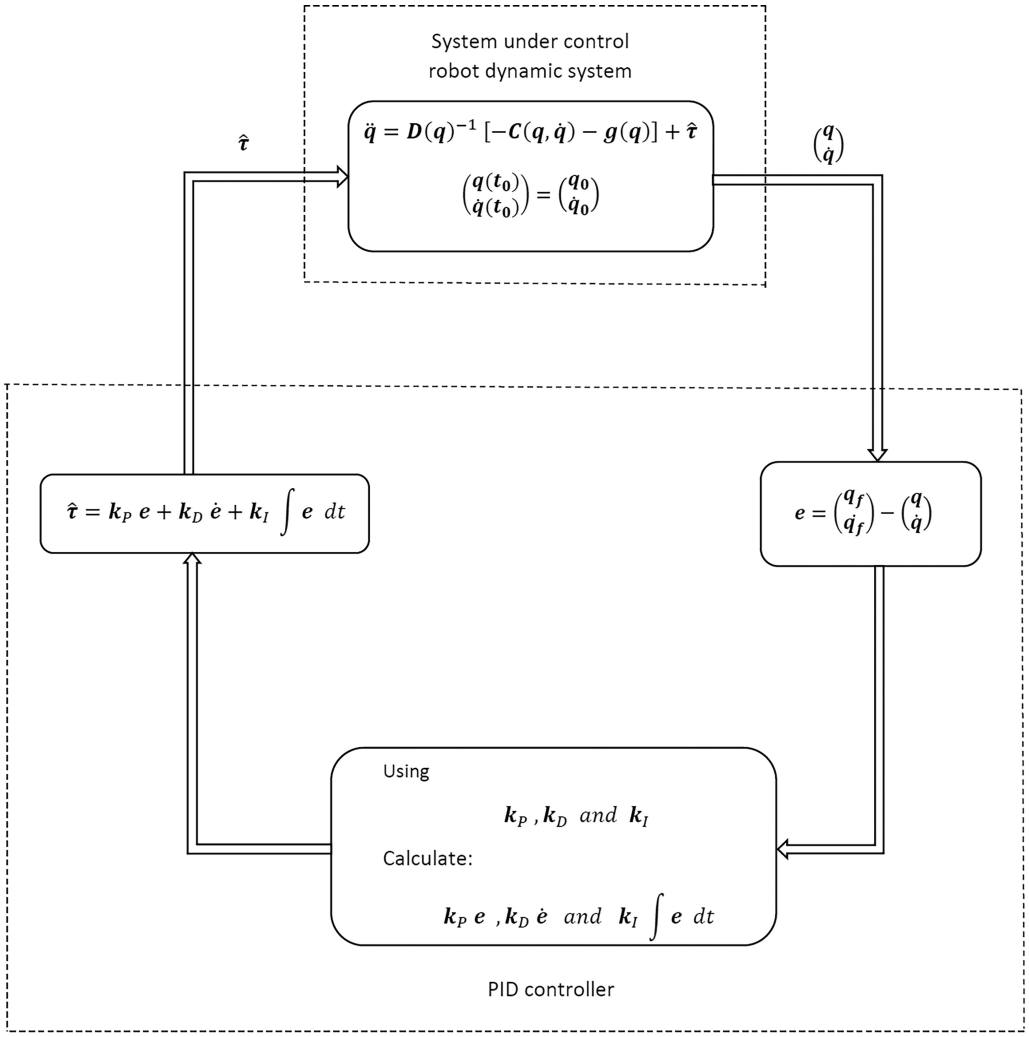

Figure 5. Block diagram for robot dynamic system using PID controller with feedback output.

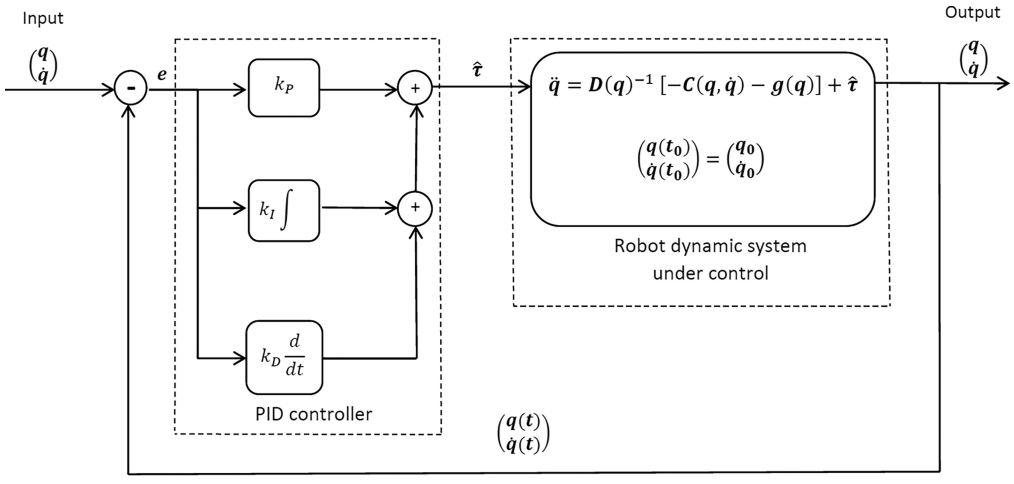

Figure 6. Block diagram of parallel PID controller for armed robot dynamic system.

is far too difficult to solve, the PID proposed controller (see Figs. 5 and 6) is used to minimise differences between the initial position and velocity and the desired ones before the given fixed time. The following explains how to combine different types of robot dynamic systems and PID controllers.

5. Combination of Robot Dynamic System and PID Controller

Considering (1) we will have

$$\ddot{q} = D^{-1}(q)[-C(q,\dot{q}) - g(q)] + \hat{\tau} \tag{7}$$

Table 4
Masses M that Added to the Last Arm in Grams (g)

M (g)	21.2	31.2	51.8	100.6	121.9	130.7	150.5	200	500	1000

where the n-vector $\widehat{\tau}$ is

$$\widehat{\tau} = D^{-1}(q)\ \tau \tag{8}$$

and the error or difference is considered as

$$e(\theta_i) = \widetilde{\theta}_i - \theta_i\ ,\quad i = 1, \ldots, n \tag{9}$$

in which $\widetilde{\theta}_i$ is the final position and θ_i is the initial position of each joint for the arm robot in radians.

From (5) and (6), the matrix form of the PID controller of each conversion function vector input $\widehat{\tau}$ is

$$\widehat{\tau} = k_P\ e + k_D\ \dot{e} + k_I\ \int e\ \mathrm{dt} \tag{10}$$

According to (10), we solve the complete system of differential equation (7) with MATLAB ode45 solver.

To determine the PID coefficients, the values k_{P_i}, k_{D_i} and k_{I_i} were manually adjusted according to the conditions defined on the robot dynamic system. These coefficients are fixed according to the increase of the robot arms in each step. In the computations here, we used

$$k_{P_i} = 30,\ k_{D_i} = 10,\ k_{I_i} = 50,\quad i = 1, 2, 3 \tag{11}$$

5.1 One-armed Robot Formulation

Now, from (7) and (10), combination for PID and dynamic system yields in

$$\begin{aligned}\ddot{\theta}_1 \ =\ & \frac{-m_1 g l_{c1} \cos(\theta_1)}{m_1 l_{c1}^2 + I_1} + k_{P_1}(\widetilde{\theta}_1 - \theta_1) + k_{D_1}\dot{\theta}_1 \\ & + k_{I_1} \int e(\theta_1)\ \mathrm{dt}\end{aligned} \tag{12}$$

The robot dynamic system with the initial condition for position $\theta_1 = \frac{-\pi}{84}$ and the final position $\widetilde{\theta}_1 = \frac{\pi}{84}$ radian with zero initial velocity for the time interval $[0, 10]$ s is considered.

5.2 Two-armed Robots Formulation

From differential equations of (3) and (7), we have

$$\begin{pmatrix}\ddot{\theta}_1 \\ \ddot{\theta}_2\end{pmatrix} = \begin{pmatrix}d_{11} & d_{12} \\ d_{21} & d_{22}\end{pmatrix}^{-1} \left[- \begin{pmatrix}\mathrm{h}\ \dot{\theta}_2 & \mathrm{h}\ \dot{\theta}_1 + h\ \dot{\theta}_2 \\ -h\ \dot{\theta}_1 & 0\end{pmatrix} \begin{pmatrix}\dot{\theta}_1 \\ \dot{\theta}_2\end{pmatrix} - \begin{pmatrix}g_1 \\ g_2\end{pmatrix} \right] + \begin{pmatrix}\widehat{\tau}_1 \\ \widehat{\tau}_2\end{pmatrix} \tag{13}$$

by placing (10) in (13) we will have

$$\begin{pmatrix}\ddot{\theta}_1 \\ \ddot{\theta}_2\end{pmatrix} = \begin{pmatrix}d_{11} & d_{12} \\ d_{21} & d_{22}\end{pmatrix}^{-1} \left[- \begin{pmatrix}\mathrm{h}\ \dot{\theta}_2 & \mathrm{h}\ \dot{\theta}_1 + h\ \dot{\theta}_2 \\ -h\ \dot{\theta}_1 & 0\end{pmatrix} \begin{pmatrix}\dot{\theta}_1 \\ \dot{\theta}_2\end{pmatrix} - \begin{pmatrix}g_1 \\ g_2\end{pmatrix} \right] + \begin{pmatrix}k_{P_1}(\widetilde{\theta}_1 - \theta_1) + k_{D_1}\dot{\theta}_1 + k_{I_1} \int e(\theta_1)\ \mathrm{dt} \\ k_{P_2}(\widetilde{\theta}_2 - \theta_2) + k_{D_2}\dot{\theta}_2 + k_{I_2} \int e(\theta_2)\ \mathrm{dt}\end{pmatrix} \tag{14}$$

For a period $[0, 10]$ s there is no velocity in the beginning time. Initial and final positions are $[\theta_1, \theta_2] = [\frac{-\pi}{84}, \frac{\pi}{84}]$ and $[\widetilde{\theta}_1, \widetilde{\theta}_2] = [\frac{\pi}{84}, \frac{-\pi}{84}]$ radian, respectively.

5.3 Three-armed Robots Formulation

The system of differential equations for (4) and (7) yields in

$$\begin{pmatrix}\ddot{\theta}_1 \\ \ddot{\theta}_2 \\ \ddot{\theta}_3\end{pmatrix} = \begin{pmatrix}d_{11} & d_{12} & d_{13} \\ d_{21} & d_{22} & d_{23} \\ d_{31} & d_{32} & d_{33}\end{pmatrix}^{-1} \left[- \begin{pmatrix}c_{11} & c_{12} & c_{13} \\ c_{21} & c_{22} & c_{23} \\ c_{31} & c_{32} & c_{33}\end{pmatrix} \begin{pmatrix}\dot{\theta}_1 \\ \dot{\theta}_2 \\ \dot{\theta}_3\end{pmatrix} - \begin{pmatrix}g_1 \\ g_2 \\ g_3\end{pmatrix} \right] + \begin{pmatrix}\widehat{\tau}_1 \\ \widehat{\tau}_2 \\ \widehat{\tau}_3\end{pmatrix} \tag{15}$$

by placing the (10) in (15) we will have

$$\begin{pmatrix}\ddot{\theta}_1 \\ \ddot{\theta}_2 \\ \ddot{\theta}_3\end{pmatrix} = \begin{pmatrix}d_{11} & d_{12} & d_{13} \\ d_{21} & d_{22} & d_{23} \\ d_{31} & d_{32} & d_{33}\end{pmatrix}^{-1} \left[- \begin{pmatrix}c_{11} & c_{12} & c_{13} \\ c_{21} & c_{22} & c_{23} \\ c_{31} & c_{32} & c_{33}\end{pmatrix} \begin{pmatrix}\dot{\theta}_1 \\ \dot{\theta}_2 \\ \dot{\theta}_3\end{pmatrix} - \begin{pmatrix}g_1 \\ g_2 \\ g_3\end{pmatrix} \right] + \begin{pmatrix}k_{P_1}(\widetilde{\theta}_1 - \theta_1) + k_{D_1}\dot{\theta}_1 + k_{I_1} \int e(\theta_1)\ \mathrm{dt} \\ k_{P_2}(\widetilde{\theta}_2 - \theta_2) + k_{D_2}\dot{\theta}_2 + k_{I_2} \int e(\theta_2)\ \mathrm{dt} \\ k_{P_3}(\widetilde{\theta}_3 - \theta_3) + k_{D_3}\dot{\theta}_3 + k_{I_3} \int e(\theta_3)\ \mathrm{dt}\end{pmatrix} \tag{16}$$

Robot dynamic system with initial condition for position $[\theta_1, \theta_2, \theta_3] = [\frac{-\pi}{84}, \frac{\pi}{84}, \frac{-\pi}{84}]$ and final position $[\widetilde{\theta}_1, \widetilde{\theta}_2, \widetilde{\theta}_3] = [\frac{\pi}{84}, \frac{-\pi}{84}, \frac{-\pi}{84}]$ radian with zero initial velocity for interval $[0, 10]$ s is considered.

5.4 Additional Mass M as a Weight

Now additional masses M will be added to the last arm as it is given in Table 4, (see also Figs. 1(b), 2(b) and 3(b)). Note that if one change the load m_i into $m_i + M$, l_i stays fixed, I_i and l_{ci} will change correspondingly. Experiments are done for different masses in Table 4, for R, RR and RRR-type manipulator robots.

6. Numerical Results

To show the effect of torque control vector $\widehat{\tau}$ in the problem described in Section 4, we proposed the following three Workexamples.

As the first Workexample, we solve the two-armed robot dynamic system (3) directly, where $[\tau_1, \tau_2] = [0.55, 0.2]$, with added mass of $M = 100.6\ g$, $t \in [0, 10]$, subject to zero initial velocity and initial position $[\theta_1, \theta_2] = [\frac{-\pi}{84}, \frac{\pi}{84}]$.

The results in Fig. 7 are computed from solving the dynamic system of the two-armed robot by determining

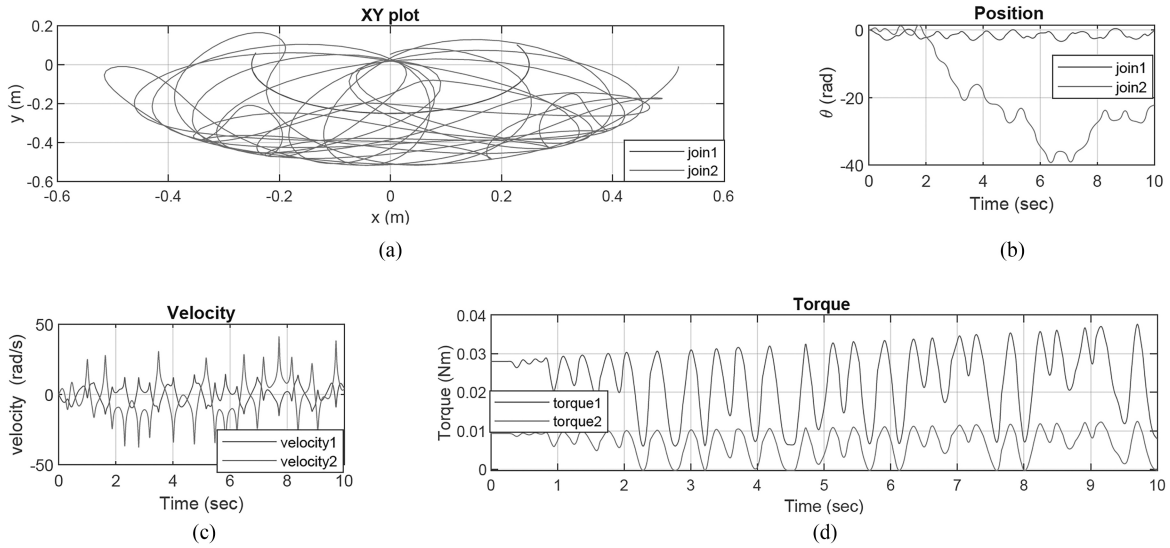

Figure 7. First Workexample; Plot of two-armed robot with payload 100.6 g: (a) plot of XY; f(b) plot of position; (c) plot of velocity; and (d) plot of torque.

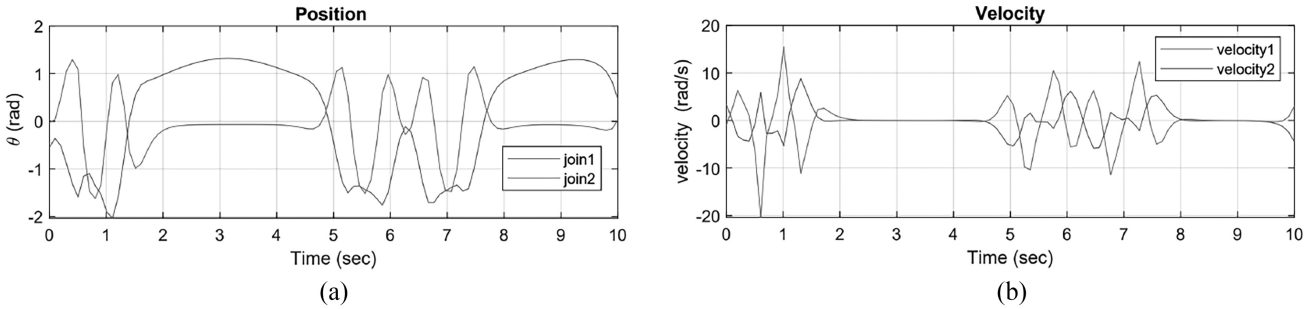

Figure 8. Second Workexample; Plots of dynamical system (3) for two-armed robot with payload 100.6 g with initial positions $[\theta_1, \theta_2] = [\frac{-\pi}{84}, \frac{\pi}{84}]$ and final positions $[\theta_{1f}, \theta_{2f}] = [\frac{\pi}{84}, \frac{-\pi}{84}]$: (a) plot of position and (b) plot of velocity.

the initial conditions on the system of equations for the robot's motion. It is shown that we have lots of fluctuations in position, velocity and torque. Thus the robot's motion in the XY plane is not reasonable (see Fig. 6).

Second Workexample; if in addition to the initial conditions $[\theta_1, \theta_2] = [\frac{-\pi}{84}, \frac{\pi}{84}]$, we add the final conditions $[\theta_{1f}, \theta_{2f}] = [\frac{\pi}{84}, \frac{-\pi}{84}]$ to the two-armed robot dynamic system (3), still we have lots of fluctuations for position and velocity (see Fig. 8), thus in practice the robot's motion is complicated.

Solving directly the first and second above Workexamples show oscillated solutions that are not usable in real-world applications. This is the motivation to write the problem described in Section 4 in the form of the following optimal control problem, third Workexamples (see (7) and (10)).

$$\begin{cases} \text{Min}_{\tau}\ J = \int_{t_0}^{t_f}\ e(\theta, \tau, t)\ \text{dt},\ \text{subject to} \\ \text{Manipulator robot dynamic system} \\ \text{for a given initial and final state vector } \theta \end{cases} \tag{17}$$

In the following subsections, three types of third Workexamples are solved successfully, using the combination of R, RR and RRR type robot dynamic systems and PID controller. As it is shown in Figs. 9–17, there is no serious oscillation for the position, torque and velocity, and the system rest before 5 s. Thus in practice, the authors recommend using the torque controlling strategy proposed by the third Workexamples.

6.1 Position Discussion for Third Workexamples

6.1.1 Robot with One Arm

According to the XY diagram (see Fig. 9), starting from a mass of 21.2 g, the amount of vertical changes is from -0.17 to -0.01 m and the horizontal changes are from 0.192 to 0.26 m, when one increases mass to 31.2 and 51.8 g, the vertical changes are still constant, but the horizontal changes shift to the right of approximately 0.002 m. With the increase of mass to 100.6 g, the vertical changes from -0.15 to 0.02 m and the horizontal changes are still shifted to the right and from 0.2495 to 0.285 m. This procedure is the same with increasing mass to 121.9, 130.7, 150.5 and 200 g, *i.e.*, the vertical changes are almost constant but it is still shifting to the right. In the masses of 500 and 1000 g, the vertical changes are from -0.1 to about 0.05 m.

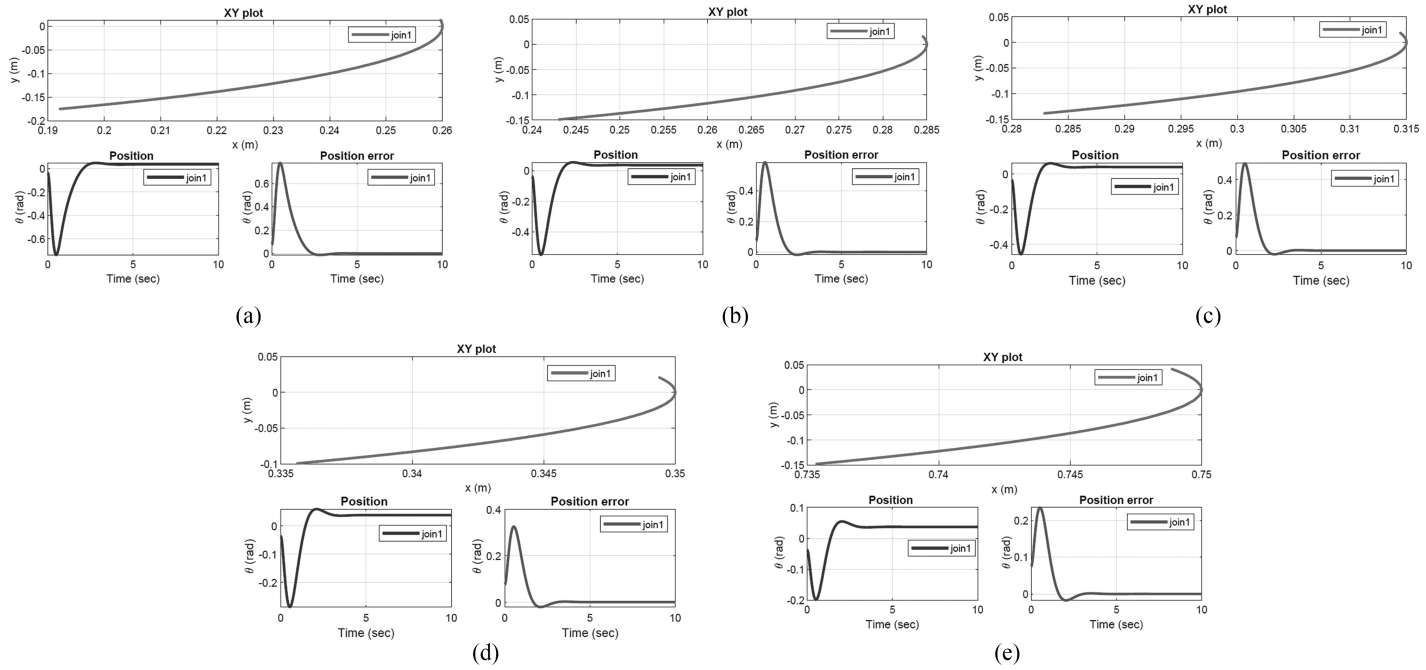

Figure 9. Plot of XY, position and position error for robot with one arm: (a) payload 21.2 g; (b) payload 100.6 g; (c) payload 150.5 g; (d) payload 500 g; and (e) payload 1000 g.

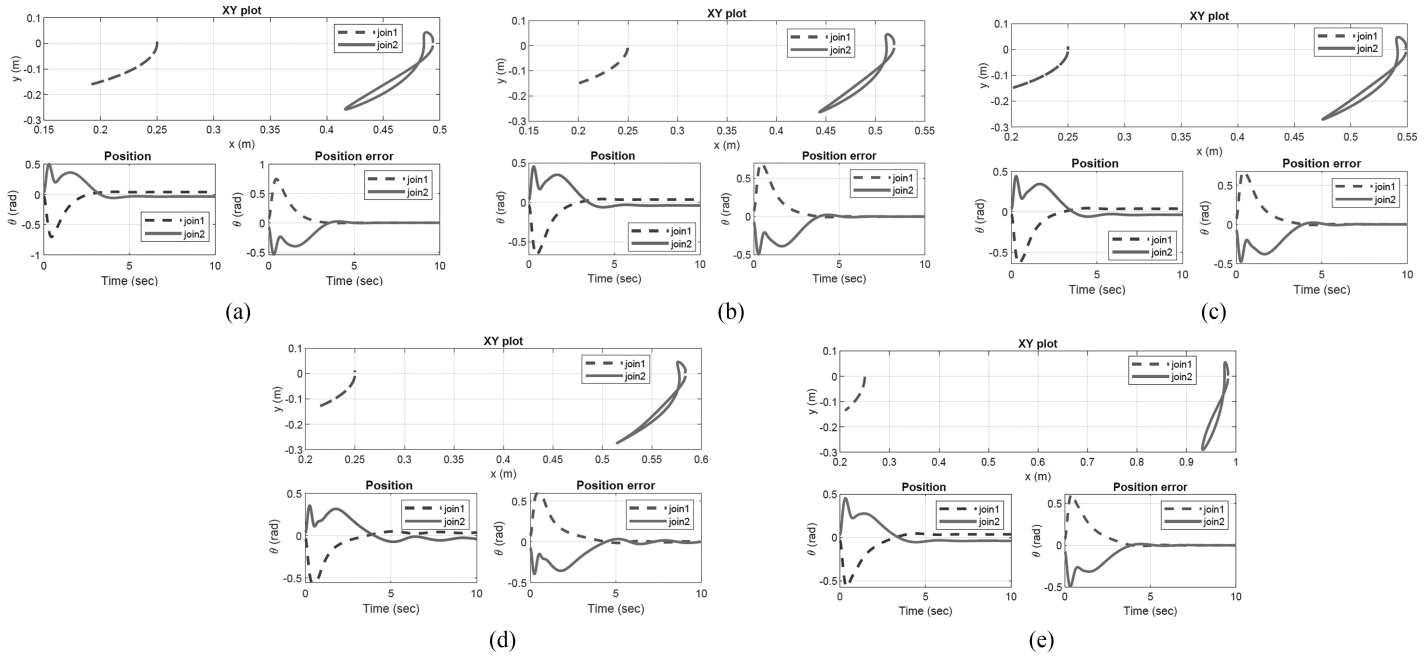

Figure 10. Plot of XY, position and position error for robot with two arms: (a) payload 21.2 g; (b) payload 100.6 g; (c) payload 150.5 g; (d) payload 500 g; (e) payload 1000 g.

The amount of horizontal changes in the mass of 200 g is approximately from 0.335 to 0.35 m. For the mass of 1000 g horizontal changes from 0.735 to 0.75 m. In masses below 100 g, the amount of vertical changes is 0.2 m and for other masses is about 0.1 m. In the position charts, it is shown that the position reaches the desired position in about 3 s. With increasing mass from 21.2 to 1000 g, the minimum position in terms of radians changes from -0.73 to -0.2 rad. The position error is also depicted in Fig. 9.

6.1.2 Robot with Two Arms

According to the XY diagram (see Fig. 10), the movement of the first arm does not change significantly when one increases the mass. The movement of the second arm increases with increasing the mass, *i.e.*, the range of horizontal and vertical changes is greater than the first arm. In the position chart, the first arm oscillates less than the second arm. In less than 1 s, the first arm has the lowest

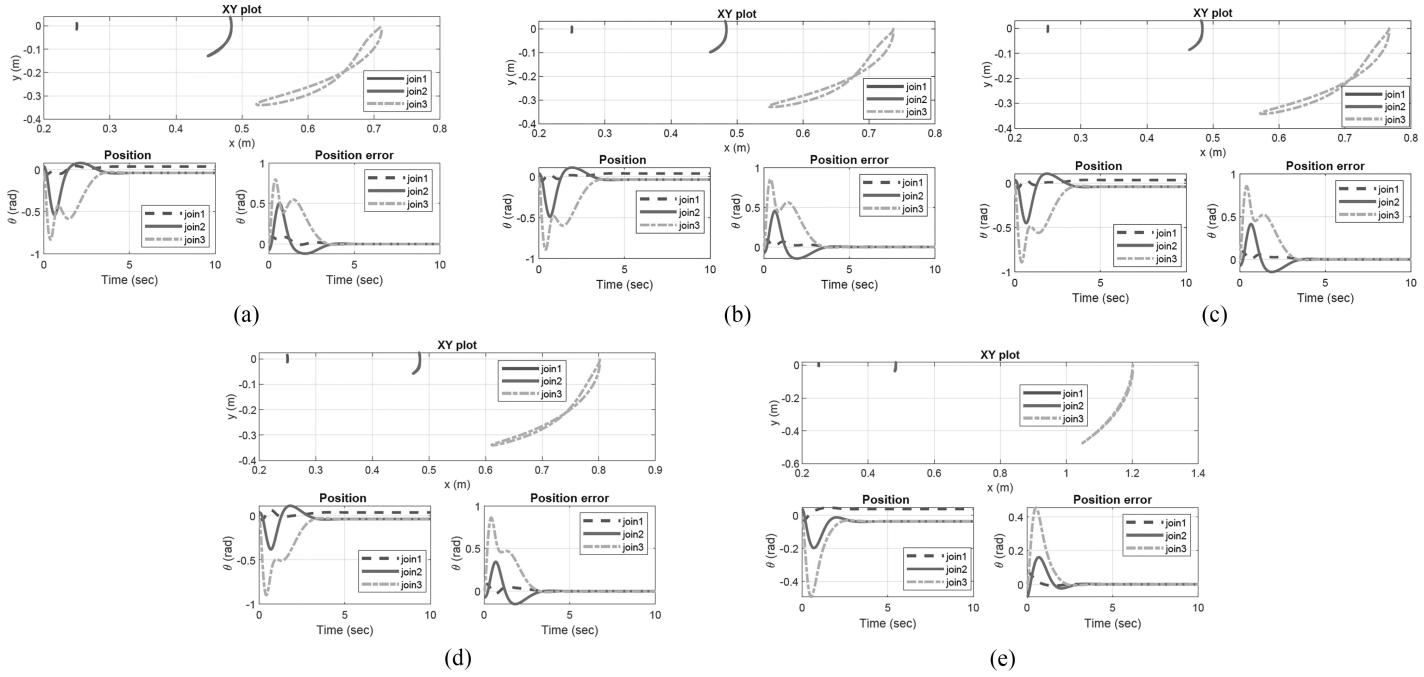

Figure 11. Plot of XY, position and position error for robot with three arms: (a) payload 21.2 g; (b) payload 100.6 g; (c) payload 150.5 g; (d) payload 500 g; (e) payload 1000 g.

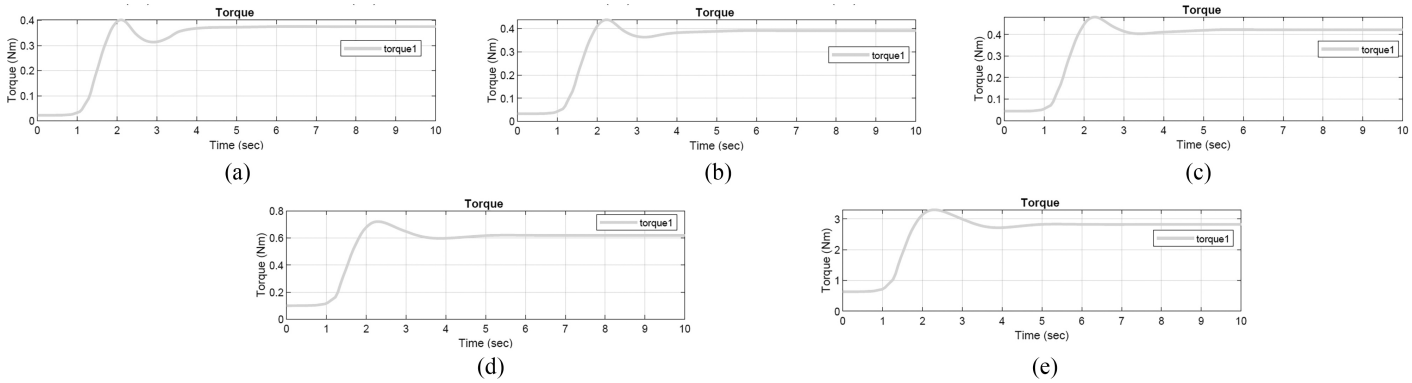

Figure 12. Plot of torque for robot with one arm: (a) payload 21.2 g; (b) payload 100.6 g; (c) payload 150.5 g; (d) payload 500 g; and (e) payload 1000 g.

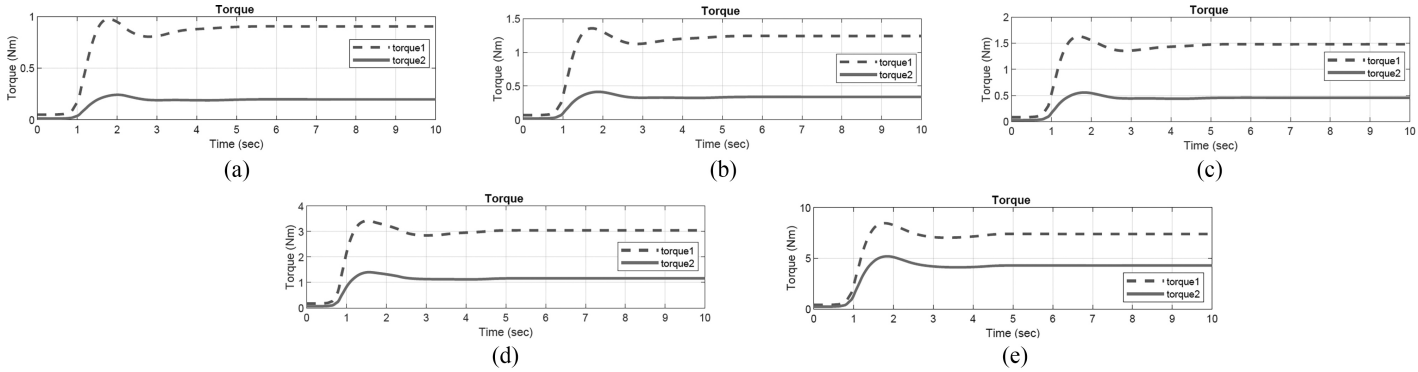

Figure 13. Plot of torque for robot with two arms: (a) payload 21.2 g; (b) payload 100.6 g; (c) payload 150.5 g; (d) payload 500 g; and (e) payload 1000 g.

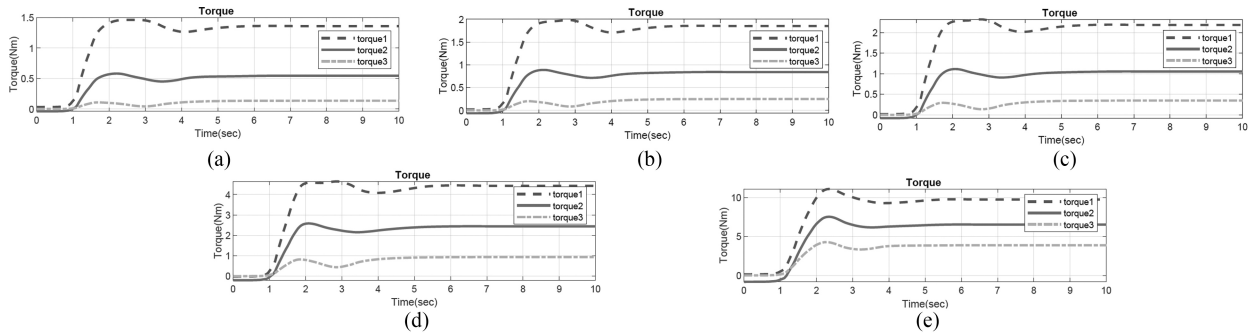

Figure 14. Plot of torque for robot with three arms: (a) payload 21.2 g; (b) payload 100.6 g; (c) payload 150.5 g; (d) payload 500 g; and (e) payload 1000 g.

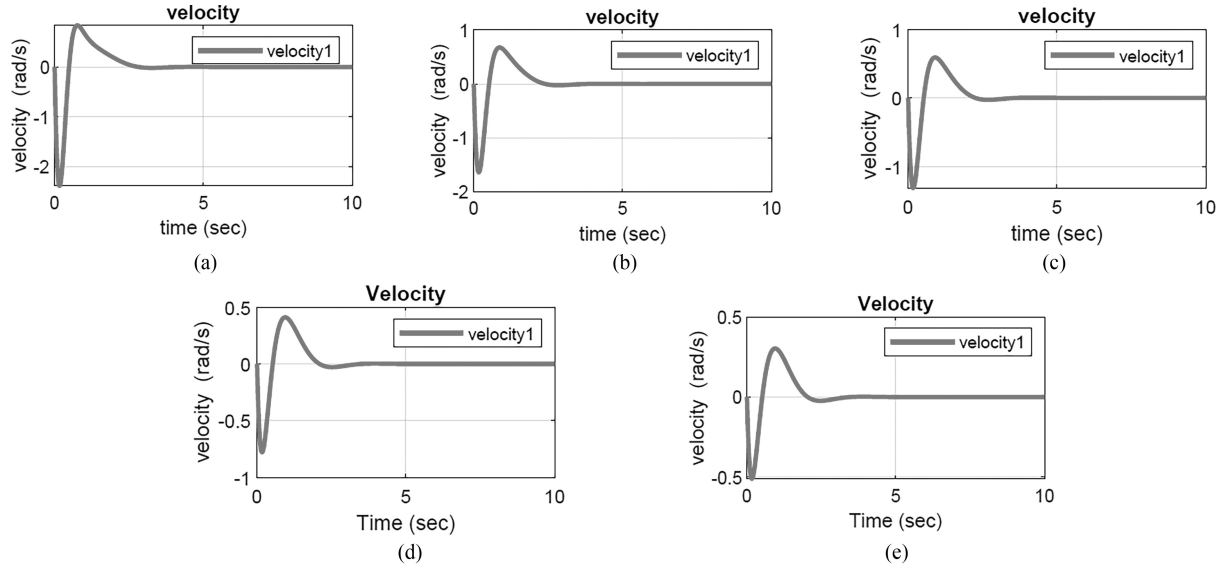

Figure 15. Velocity plots for robot with one arm: (a) payload 21.2 g; (b) payload 100.6 g; (c) payload 150.5 g; (d) payload 500 g; and € payload 1000 g.

position and the second arm is at its highest position. The first and second arms achieve the rest in almost 5 s. The range of motion changes does not change significantly with increasing mass.

6.1.3 Robot with Three Arms

According to the XY chart (see Fig. 11), the amount of movement of the first arm is very low and has a small range of motion. The change in motion in the horizontal direction is about 0.001 m and in the vertical direction is about 0.02 m. The range of motion for second arm is in the range between 0.44 to 0.48 m in the horizontal direction and from -0.12 to 0.03 m in the vertical direction. Not very much, but the third arm has a greater range of motion in the horizontal and vertical directions than the first two arms. From the mass of 21.2 to 200 g, the amount of horizontal and vertical changes is small, but for the mass of 500 and 1000 g, the range of motion from the horizontal direction varies from 0.6 to 0.08 m. In the position diagram, the first, second and third arms have no more than one oscillation before going the rest for $t = 4$ s.

6.2 Torque Commentation for Third Workexamples

6.2.1 Robot with One Arm

In the torque diagram (see Fig. 12), it is shown that one does not need any torque after almost 4 s. After 1 s, torque peaks and reaches 0.4 Nm for a mass of 21.2 g, and this value increases to 0.5 Nm for a mass of 200 g; for a mass of 500 and 1000 g it increases to point 0.7 and 3 Nm, respectively. Torque decreases after nearly 3 s until it rises again in 4 s and then stabilises.

6.2.2 Robot with Two Arms

In the torque diagram (see Fig. 13), the amplitude of changes for first arm is greater than the second arm. For masses below 100 g, the maximum arm torque is between 1 and 1.1 Nm, and for masses up to 200 g, this value increases to 2 Nm, for masses of 500 g, it is about 3.5 Nm, and for masses of 1000 g, this value is 9 Nm. Up to 1 s the torque is constant and the maximum value occurs between 1 and 2 s and is stable from 3 s onwards. The torque of

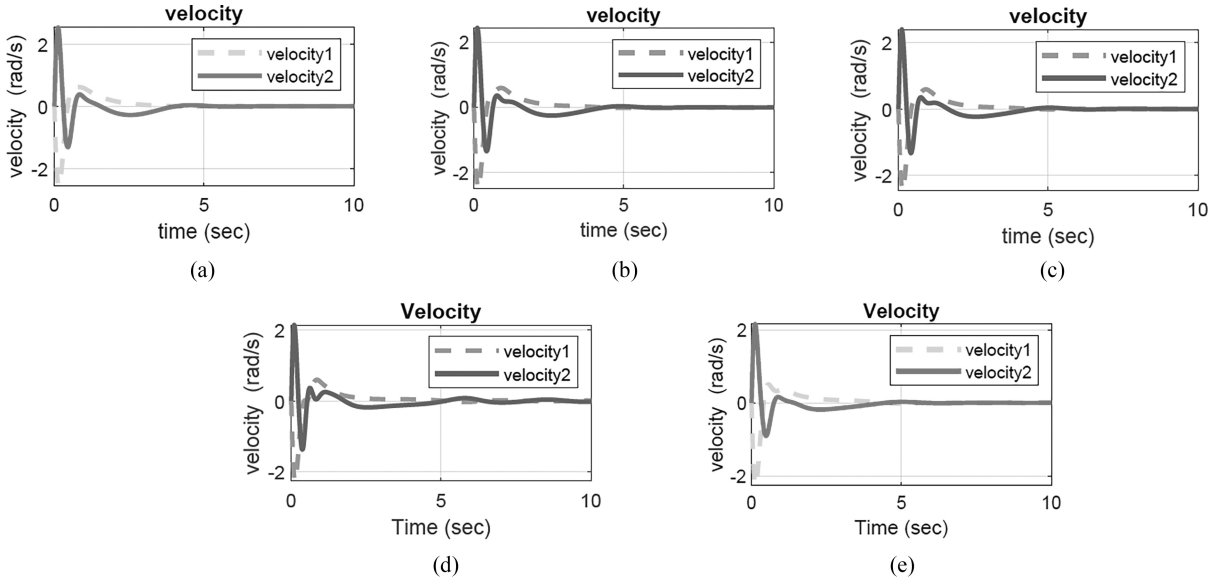

Figure 16. Plot of velocity for robot with two arms: (a) payload 21.2 g; (b) payload 100.6 g; (c) payload 150.5 g; (d) payload 500 g; and (e) payload 1000 g.

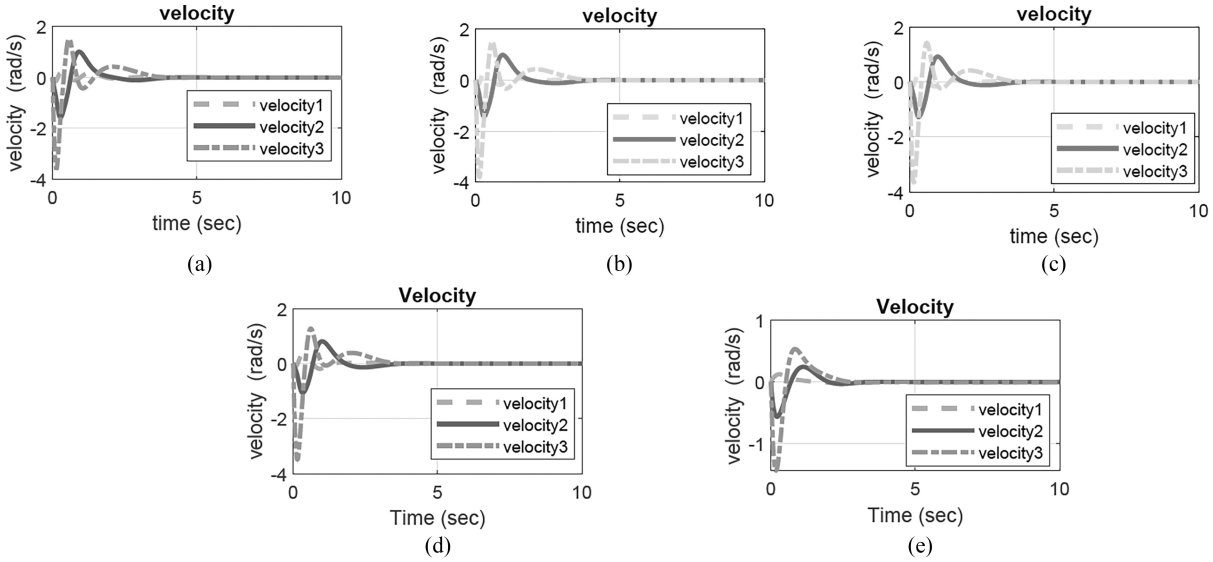

Figure 17. Plot of velocity for robot with three arms: (a) payload 21.2 g; (b) payload 100.6 g; (c) payload 150.5 g; (d) payload 500 g; and (e) payload 1000 g.

the second arm for mass less than 100 g is at a maximum value of about 0.125 Nm and with increasing mass this value increases to 0.5 Nm and for mass 500 and 1000 g is 1 and 5 Nm. For both arms, the maximum amount of torque occurs between 1 and 2 s. The system takes a rest after almost 4 s.

6.2.3 Robot with Three Arms

In the torque diagram (see Fig. 14), the first and third arms have the highest and lowest torque amounts. In all experiments, torque rests before 5 s. For the mass of 1000 g, one needs more torque amount but less time to take the rest. For masses below 100 g, the maximum torque of the first arm is about 1.5 Nm and with increasing mass up to 200 g it becomes about 2.5 Nm. For a mass of 500 g, it is 4.5 Nm and for a mass of 1000 g, it is about 10.1 Nm. Regarding the torque values, the behaviour pattern states the same for three different arms. More payloads need more torques as expected.

6.3 Velocity Dissection for Third Workexamples

6.3.1 Robot with One Arm

As it is shown in Fig. 15, velocity is in a steady state after about 3 s. For a mass of 21.2 g in 0.1 s lowest velocity -2.3 $\frac{\text{rad}}{s}$ and highest velocity 0.8 $\frac{\text{rad}}{s}$ in 0.7 s happens. As the mass increases, the velocity changes amplitude decreases.

6.3.2 Robot with Two Arms

In the velocity diagram (see Fig. 16), velocity changes amplitude for both arms are almost in the same range. The velocity takes the rest before 10 s for all payloads. According to the initial and final positions defined in the problem, the first arm has a negative velocity and the second arm has a positive velocity. Thus, in 0.1 s, the first arm has the lowest speed and the second arm has the highest value. Then the first arm reaches its maximum again in 0.7 s and the second arm in 0.8 s has its maximum. Both arms move together again until they take a rest in 4 s. In the period of 0.3 to 4 s, the speed of the first arm is faster than the second arm.

6.3.3 Robot with Three Arms

As it is shown in the velocity diagram (see Fig. 17), there is no motion after almost 4 s. For a mass of 1000 g, this happens sooner in almost 3 s. The first arm has the lowest speed range and the third arm has the highest speed range. For a mass of 1000 g, the speed changes range is less than the other payloads while the speed is higher.

7. Conclusion

Direct solving the dynamical system (3) (see first and second Workexamples, Figs. 7 and 8, respectively) of transporting some payloads from the initial position to the final position gives a very oscillated solution that is not usable in real-world applications. We have shown that by combining PID controller and dynamic system for manipulator robots of different types and different weights, we will be able to solve the problem in the type of optimal control problem successfully (see third Workexamples, Figs. 9–17). This concludes that optimal torque control has a great effect on the well-done operation for this kind of payload transportation.

References

[1] A. Bayram and A S. Duru, Design and control of a rehabilitation robot manipulator for head-neck orthopaedic disorders, *International Journal of Robotics and Automation, 37*(6), 2022, 486–497.

[2] E. Lyu, X. Yang, W. Liu, J. Wang, S. Song, and M. Q.-H. Meng, An autonomous eye-in-hand robotic system for picking objects in a supermarket environment with non-holonomic constraint, *International Journal of Robotics and Automation, 37*(4), 2022.

[3] L.A Nguyen, T.D Ngo, T.D Pham and X.T. Truong, An efficient navigation system for autonomous mobile robots in dynamic social environments, *International Journal of Robotics and Automation*, *37*(1) 2022, 97–106.

[4] A. Malek, L. Jafarian-Khaled Abad, and S. Khodayari-Samghabadi, Semi-infinite programming to solve armed robot trajectory problem using recurrent neural network, *International Journal of Robotics and Automation, 30*(2), 2015, 113–118.

[5] G. Zhong, C. Wang, and W. Dou, Fuzzy adaptive PID fast terminal sliding mode controller for redundant manipulator, *Mechanical Systems and Signal Processing 159*, 2021, 107577

[6] H.R. Nohooji, Constrained neural adaptive PID control for robot manipulators, *Journal of the Franklin Institute, 357*(7), 2020, 3907–3923.

[7] I. Gandarilla, V. Santibanez, J. Sandoval, and J G. Romero, PID passivity-based control laws for joint position regulation of a self-balancing robot, *Control Engineering Practice, 116*, 2021, 104927

[8] X. Zhang, H. Li, G. Li, T. Chen, and J. Shan, Continuous PID-SMC based on improved EHGO for robot manipulators with limited state measurements, *Journal of the Franklin Institute, 357*, 2020, 10648–10668.

[9] P.N. Paraskevopoulos, *Modern control engineering*, Boca Raton, FL: CRC Press, 2001

[10] B.A. Francis and W.M. Wonham, The internal model principle of control theory, *Automatica, 12*, 1976, 457–465.

[11] B Zhu, L Wang, J Wu, and Q Li, Optimization design and performance comparison of two 5-DOF parallel manipulators used for loading device, *International Journal of Robotics and Automation, 37*(4), 2022

[12] M.W. Spong, S. Hutchinson, and M. Vidyassagar, *Robot modeling and control*, Hoboken, NJ: Wiley, 2006

[13] A. Gallant and C. Gosselin, Extending the capabilities of robotic manipulators using trajectory optimization, *Mechanism and Machine Theory, 121*, 2018, 502–514.

[14] J. Angeles, *Fundamentals of robotics mechanical system*, Cham: Springer, 2014

[15] T. Bajd, M. Mihelj, J. Lenarcic, A. Stanovnik, and M. Munih, *Robotics*, Berlin: Springer Verlag, 2010

[16] Z. Qi, Z. Dan, Z. Shuo, L. Xueling, and H. Guanyu, Structural design and kinematic analysis of a group of translational parallel mechanisms, *International Journal of Robotics and Automation*, *37*(4), 2022, 382–390.

Biographies

Alaeddin Malek received the M.Sc. degree in applied mathematics from McGill University, Canada, in 1986, and the Ph.D. degree in applied mathematics from the University of Wales, U.K., in 1991. He is an Associate Professor with the Applied Mathematics Department, Tarbiat Modares University, Tehran, Iran. His research interests are neural networks, optimisation, robotics, control theory and numerical solutions for PDEs.

Farideh Giv received the B.Sc. degree in applied mathematics from Damghan University, Damghan, Iran, in 2009, and the M.Sc. degree in applied mathematics from Semnan University, Semnan, Iran, in 2014. She is currently pursuing the Ph.D. degree with Tarbiat Modares University, Tehran, Iran. Her interests include numerical solutions for robotics problems and control theory.